Protein Science (1999), *8*:2630–2638. Cambridge University Press. Printed in the USA.

Three-dimensional solution structure of mouse [Cd_7]-metallothionein-1 by homonuclear and heteronuclear NMR spectroscopy

KLAUS ZANGGER,[1] GÜLIN ÖZ,[1] JAMES D. OTVOS,[2] AND IAN M. ARMITAGE[1]

[1]Department of Biochemistry, Molecular Biology and Biophysics, University of Minnesota, Minneapolis, Minnesota 55455
[2]Department of Biochemistry, North Carolina State University, Raleigh, North Carolina 27695

(RECEIVED May 20, 1999; ACCEPTED September 9, 1999)

Abstract

Sequential ^{1}H-NMR assignments of mouse [Cd_7]-metallothionein-1 (MT1) have been carried out by standard homonuclear NMR methods and the use of an accordion–heteronuclear multiple quantum correlation (HMQC) experiment for establishing the metal, $^{113}Cd^{2+}$, to cysteine connectivities. The three-dimensional structure was then calculated using the distance constraints from two-dimensional nuclear Overhauser effect (NOE) spectroscopy spectra and the Cys–Cd connectivities as input for a distance geometry-dynamical simulated annealing protocol in X-PLOR 3.851. Similar to the mammalian MT2 isoforms, the homologous primary structure of MT1 suggested two separate domains, each containing one metal cluster. Because there were no interdomain constraints, the structure calculation for the N-terminal β- and the C-terminal α-domain were carried out separately. The structures are based on 409 NMR constraints, consisting of 381 NOEs and 28 cysteine–metal connectivities. The only elements of regular secondary structure found were two short stretches of 3_{10} helices along with some half-turns in the α-domain. Structural comparison with rat liver MT2 showed high similarity, with the β-domain structure in mouse MT1 showing evidence of increased flexibility compared to the same domain in MT2. The latter was reflected by the presence of fewer interresidue NOEs, no slowly exchanging backbone amide protons, and enhanced cadmium–cadmium exchange rates found in the β-domain of MT1.

Keywords: ^{113}Cd; 2D NMR; accordion-HMQC; mouse metallothionein-1; nuclear magnetic resonance; structure

Metals are both essential and toxic elements to life processes. On the one hand, they are integral, functional components of many enzymes and transcriptional regulatory proteins, while on the other hand, the binding of nonnative metals to biological macromolecules may perturb their function and metal-catalyzed formation of oxygen-derived free radicals has been implicated in a wide variety of pathological conditions such as mutagenicity and carcinogenicity. To cope with potentially hazardous levels of heavy metal ions, organisms appear to have developed an integrated, metal-regulatory network to control the concentration and availability of these elements. One of the components of this network is metallothionein (MT), a small (<7 kDa) protein with a high cysteine content (~30%) and the highest known metal content after ferritins. Metallothioneins bind both essential (Cu^{1+} and Zn^{2+}) and nonessential (Cd^{2+} and Hg^{2+}) metals. Metal coordination in MT has a high thermodynamic but low kinetic stability. Thus, metal binding is very tight, but there is facile metal exchange with other proteins. MTs are thought to function biologically as intracellular distributors and mediators of the metals they bind (Kägi & Kojima, 1987; Kägi & Schäffer, 1988). MTs are ubiquitous proteins, found in animals, higher plants, eukaryotic organisms, and some prokaryotes. In animals, the two major metallothionein isoforms, MT1 and MT2, are most abundant in parenchymatous tissues, i.e., liver, kidney, pancreas, and intestines, but their occurrence and biosynthesis have been documented in many tissues and cell types. These two isoforms were initially distinguished by their elution profiles from anion exchange columns due to the presence of an extra negative charge in MT2. In addition to the charges from the seven metal ions and the 20 thiolate sulfurs, mammalian MT1s have two negatively charged and seven positively charged residues, while MT2s have amino acid side chains carrying four negative and eight positive charges. The functional discrimination between the two isoforms is unknown, although a recent phylogenic analysis of their gene sequences (Binz & Kägi, 1999) revealed that the introns and 5′ untranslated regions of the two genes and more importantly, the 5′ untranscribed regions that contain the regulatory elements, are different in MT1 vs. MT2. These differences result in differential tissue specific regulation of the two isoforms.

Reprint requests to: Ian M. Armitage, University of Minnesota, Department of Biochemistry, Molecular Biology and Biophysics, 6-155 Jackson Hall, 321 Church Street S.E., Minneapolis, Minnesota 55455; e-mail: armitage@bscl.msi.umn.edu.

Abbreviations: COSY, correlation spectroscopy; HMQC, heteronuclear multiple quantum correlation; HSQC, heteronuclear single quantum correlation; IPTG, isopropyl-βD-thiogalactoside; MT, metallothionein; NOE, nuclear Overhauser effect; NOESY, NOE spectroscopy; RMSD, root-mean-square deviation; TOCSY, total correlation spectroscopy.

Thus far, structural investigations of mammalian metallothioneins have been limited to MT2s from various sources (Arseniev et al., 1988; Schultze et al., 1988; Messerle et al., 1990b). The only MT1 isoform that has been structurally characterized is the crustaceous MT1 from the blue crab *Callinectes sapidus* (Narula et al., 1995). Invertebrate MTs have little sequence homology (~35%) to mammalian MTs, and no structural conclusions about mammalian MT1s can be drawn from the crab MT1 structure. Mammalian MT1 and MT2s, on the other hand, have high sequence homology (~85%), and the determination and comparison of the structure and metal binding properties of the two isoforms are necessary prerequisites to understanding possible functional consequences of the existence of multiple isoforms.

In this paper, we present the first report of the tertiary structure of a mammalian MT1 isoform. The sequential ^{1}H-NMR assignments and structure determination were performed on mouse (*Mus musculus*) [Cd_7]-metallothionein-1 by homonuclear and heteronuclear NMR spectroscopy. As will be shown, the structure of mouse MT1 is similar to mammalian MT2s. It is a dumbbell-shaped protein with seven cadmium ions located in two separate clusters. The tertiary structure is determined mainly by the coordination of the metal ions by the thiolates of the 20 cysteine residues. The only elements of regular secondary structure are two short stretches of 3_{10} helices along with some half-turns.

Results

Resonance assignments

Sequential ^{1}H-NMR assignments were accomplished by standard procedures as described in the literature (Wüthrich, 1986). TOCSY spectra, with mixing times of 30 and 60 ms, were used to assign individual spin systems, and assigned residues were identified with respect to their position within the protein by sequential NOEs. The fingerprint region of a TOCSY spectrum is shown in Figure 1. To slow down amide proton and conformational (cadmium–cadmium) exchange, spectra were acquired at 10 °C and a pH of 6.5. To resolve some overlapped resonances, a set of spectra was also acquired at 25 °C. The intensity of the cross peaks was on average much higher for residues in the α-domain, where 278 NOEs could be extracted compared with just 103 in the β-domain, which would be consistent with a more flexible structure for this latter domain. Although all the resonances could be observed for the C-terminal domain, NH cross peaks from two residues in the N-terminal domain (Cys7 and Cys13) could not be found in any of the spectra. A list of chemical shifts is available as Supplementary material in the Electronic Appendix.

Secondary structural analysis

A graphical representation of the sequential and medium-range NOEs, which indicate regular secondary structural elements, is shown in Figure 2. As is immediately obvious, there are no α-helices or β-sheets in mouse MT1, only a short stretch of a 3_{10} helix, which can be identified between residues 42 and 47 by the presence of $d_{NN}(i,i+2)$ and $d_{\alpha N}(i,i+2)$ NOEs. Another 3_{10} helix is indicated for the last five C-terminal residues where in addition to the $d_{NN}(i,i+2)$ and $d_{\alpha N}(i,i+2)$ connectivities, we found NOEs between the α-proton of threonine-58 and the amide and the β-proton of cysteine-61 (not shown). Several NOE signatures indicative of either type II turns or half-turns are evident as well, as indicated in Figure 2. These putative turns are characterized by a strong

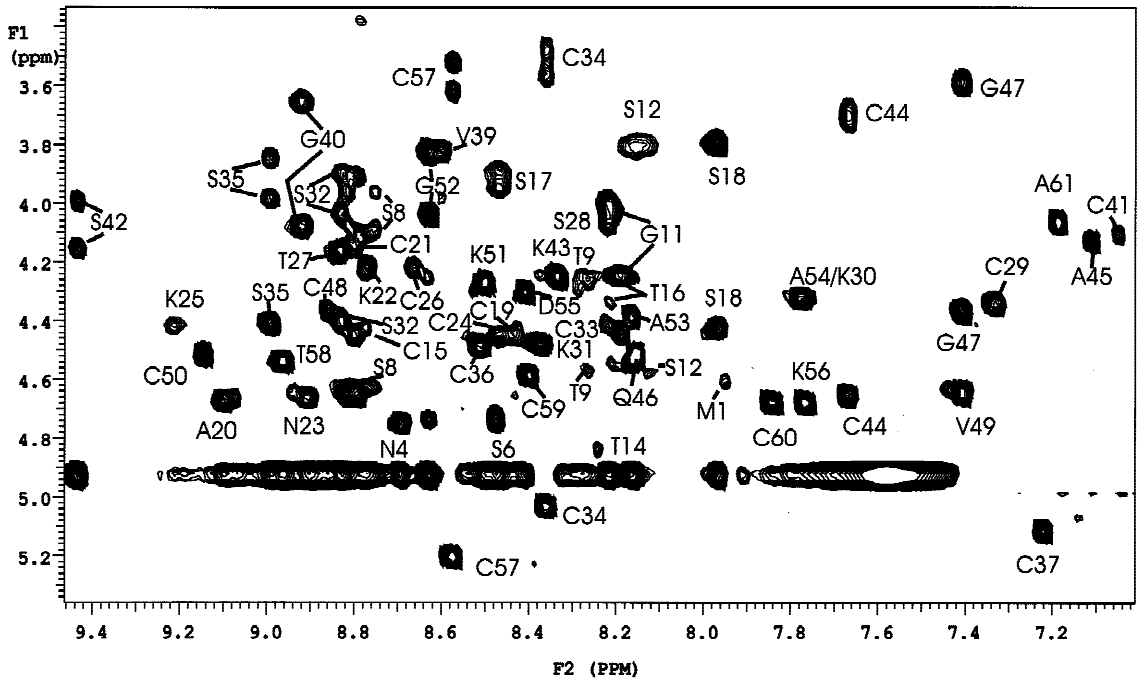

Fig. 1. Fingerprint region of the 800 MHz TOCSY spectrum recorded with a 60 ms mixing time on a 0.7 mM sample of mouse Cd_7 MT1 at 10°C and pH 6.5. Thirty-two transients were acquired for each of the 256 increments. The amino acid type and sequence number of each cross peak is indicated.

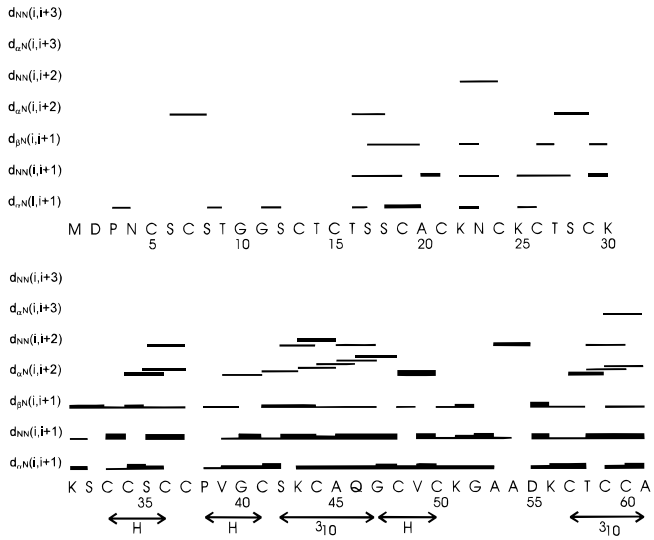

Fig. 2. Amino acid sequence and summary of sequential NOEs indicative of secondary structural elements. The thickness of the lines corresponds to the intensity of the NOE. The location of half-turns (H) and 3_{10} helical segments (3_{10}) are indicated below the sequence.

$d_{\alpha N}(i, i+1)$ connectivity between the second and third residue in the turn, as well as a strong $d_{NN}(i, i+1)$ interaction between the third and the fourth amino acid and medium $d_{\alpha N}(i, i+1)$ connectivities between all four residues in the turn. The fewer NOEs in the β-domain preclude the assignment of any secondary structural elements in this domain. In addition to the NOEs shown in Figure 2, a significant number of other NOEs (e.g., $d_{\alpha N}(i, i-1)$, $d_{\alpha N}(i, i-2)$, and α-proton to side chain) where found, which corroborated or for some residues enabled the full sequential assignments in both domains.

Structure

A total of 381 NOEs were used for the structure calculation, of which 28 were long-range constraints ($d_{ij}, j > i+4$) (Table 1). The number of intra-residue, inter-residue, and long-range NOEs is shown graphically in Figure 3. The cadmium–cysteine connectivities that were obtained by an accordion-HMQC experiment were crucial for the definition of the three-dimensional structure. The ^{1}H-^{113}Cd accordion HMQC spectrum as well as a graphical depiction of the cysteine–cadmium connectivities in relation to the primary amino acid sequence are shown in Figure 4. As was found with the mammalian MT2s, the metals are bound in two distinct metal clusters in separate protein domains with no interdomain NOEs. The structure calculations were therefore carried out separately for the two domains, as described in Materials and methods. The N-terminal β-domain includes residues 1–30, with residues 31–61 belonging to the C-terminal α-domain. The structures that showed not more than one NOE violation greater than 0.5 Å, an RMS difference for bond deviations from ideality of less than 0.01 Å, and an RMS difference for angle deviations from ideality of $<5°$ were selected and are shown in Figure 5 as a least-squares superposition of structures. As expected, the β-domain with fewer NOE constraints is not as well defined as the α-domain, as a result of greater flexibility of the N-terminal domain. A summary of the structural statistics for both domains is shown in Table 2, with an RMSD of backbone atoms of just 0.78 Å for the α-domain compared to 1.92 Å in the β-domain. The structures will be deposited at the Brookhaven Protein Data Bank, and the chemical shifts at the BioMagResBank.

Table 1. *Long-range NOEs between protons at least five residues apart (d_{ij}; $j > i + 4$)*

Long-range NOEs
β-Domain
Asn4(α) ---------- Lys22(β)
Asn4(α) ---------- Asn23(NH)
Asn4(β) ---------- Asn23(NH)
Cys5(α) ---------- Cys21(β)
Cys5(β) ---------- Cys21(β)
Asn23(β) --------- Cys29(α)
α-Domain
Lys31(NH) ------ Val39(γ)
Lys31(α) --------- Val39(γ)
Ser32(β) --------- Val39(β)
Ser32(NH) ------- Val39(γ)
Cys33(NH) ------ Val39(γ)
Cys33(α) --------- Cys48(β)
Cys33(β) --------- Cys48(NH)
Ser35(β) --------- Asp55(NH)
Cys36(α) --------- Asp55(NH)
Cys36(α) --------- Asp55(α)
Cys36(α) --------- Lys56(NH)
Cys36(β) --------- Lys56(NH)
Cys36(β) --------- Lys56(α)
Cys36(α) --------- Cys57(NH)
Cys36(β) --------- Cys57(NH)
Cys36(β) --------- Cys57(α)
Cys36(β) --------- Cys57(β)
Lys43(β) --------- Val49(γ)
Lys43(γ) --------- Val49(γ)
Lys43(γ) --------- Cys60(α)
Cys44(NH) ------ Val49(γ)
Val49(γ) --------- Cys59(β)

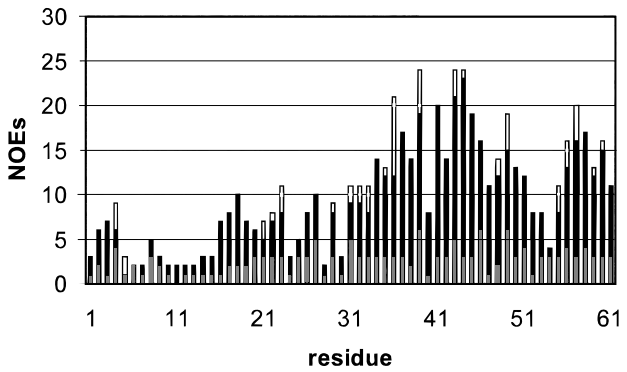

Fig. 3. Bar diagram of NOEs per residue along the peptide chain of mouse [Cd_7]-MT1. Shading representing intraresidue NOEs is gray, that for short and medium-range NOEs is black, and long-range NOEs (d_{ij}; $j > i + 4$) are shown in white.

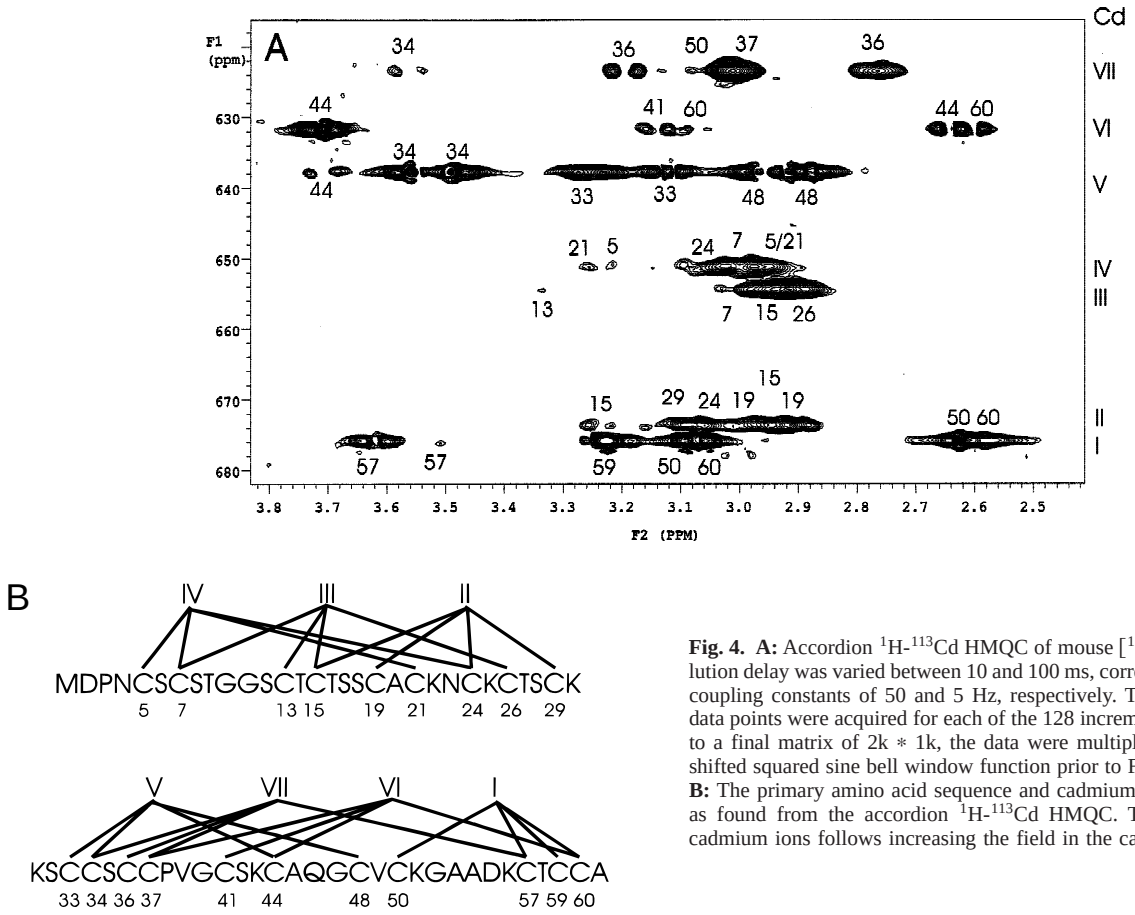

Fig. 4. **A:** Accordion ^{1}H-^{113}Cd HMQC of mouse [$^{113}Cd_7$]-MT1. The evolution delay was varied between 10 and 100 ms, corresponding to ^{1}H-^{113}Cd coupling constants of 50 and 5 Hz, respectively. Thirty-two scans of 2k data points were acquired for each of the 128 increments. After zero filling to a final matrix of 2k ∗ 1k, the data were multiplied with a 60° phase-shifted squared sine bell window function prior to Fourier transformation. **B:** The primary amino acid sequence and cadmium–proton connectivities as found from the accordion ^{1}H-^{113}Cd HMQC. The numbering of the cadmium ions follows increasing the field in the cadmium spectrum.

Chemical exchange

Two kinds of chemical exchange phenomena were studied in mouse MT1, amide proton exchange rates, and cadmium–cadmium exchange. Both of these exchange mechanisms have been described for the structurally characterized MT2 isoforms (Otvos et al., 1987; Messerle et al., 1990a, 1992), and therefore allowed a quantitative comparison of the flexibility of mouse MT1 with

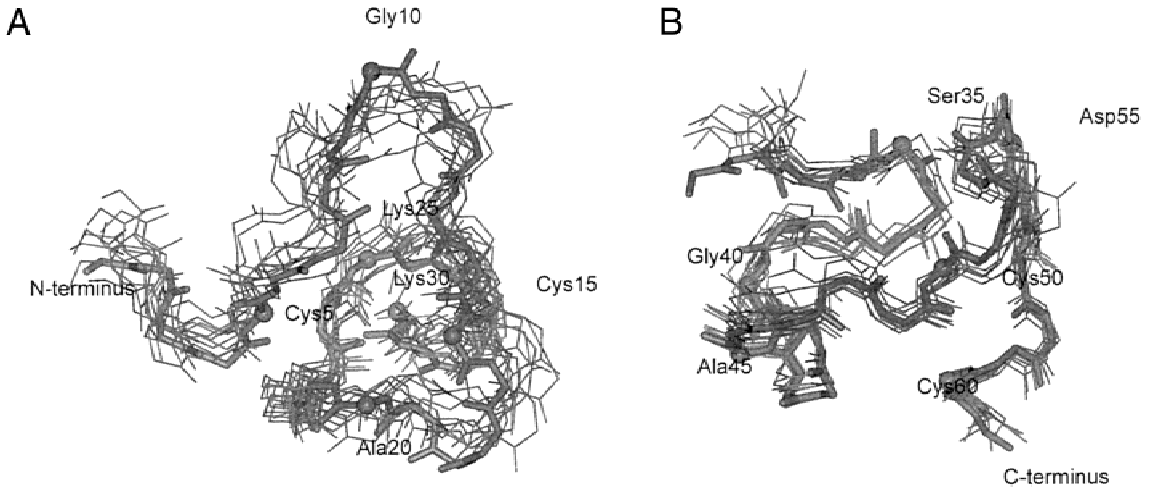

Fig. 5. Least-squares superposition of the backbones of the 10 lowest energy structures of (**A**) the β- and (**B**) the α-domain of mouse [Cd_7]-MT1. The thick lines represent the energy-minimized average structure. The α-carbon of every fifth residue is shown as a ball for easier orientation.

Table 2. *Structural characteristics of both domains of mouse MT1*[a]

Structural statistics[b]	⟨SA⟩	⟨SA⟩$_{av}$
β-Domain (residues 1–30)		
Energies (kcal/mol)		
$E_{overall}$	208.6 ± 26.9	187.4
E_{bonds}	8.85 ± 1.28	8.86
E_{angles}	118.2 ± 14.7	101.6
E_{vdW}	14.1 ± 5.0	10.45
RMSDs from idealized covalent geometry used within X-PLOR		
Bonds (Å)	0.0047 ± 0.0003	0.0047
Angles (deg)	1.65 ± 0.13	1.47
Impropers (deg)	0.73 ± 0.08	0.62
NOEs (Å)	0.101 ± 0.009	0.103
Atomic RMS differences ⟨SA⟩ vs. ⟨SA⟩$_{av}$		
All atoms except hydrogen (Å)	2.422	
Backbone atoms (Å)	1.918	
α-Domain (residues 31–61)		
Energies (kcal/mol)		
$E_{overall}$	379.6 ± 38.6	414.4
E_{bonds}	23.40 ± 2.50	23.28
E_{angles}	188.4 ± 25.5	217.3
E_{vdW}	30.90 ± 9.60	43.01
RMSDs from idealized covalent geometry used within X-PLOR		
Bonds (Å)	0.0075 ± 0.0004	0.0075
Angles (deg)	2.17 ± 0.15	2.31
Impropers (deg)	0.70 ± 0.06	0.74
NOEs (Å)	0.094 ± 0.005	0.091
Atomic RMSD ⟨SA⟩ vs. ⟨SA⟩$_{av}$		
All atoms except hydrogen (Å)	1.327	
Backbone atoms (Å)	0.780	

[a] ⟨SA⟩ refers to 10 simulated annealed structures that do not have more than 1 NOE violations >0.5 Å, an RMSD for bonds of <0.01 Å, and an RMSD for angles of <5°. ⟨SA⟩$_{av}$ is the energy-minimized average structure of the 10 best structures. Only the backbone atoms were used for the best-fit superposition.

[b] None of the selected structures exhibited more than 1 NOE-derived distance violations of >0.5 Å or backbone dihedral violations of >5°. Energies were calculated by X-PLOR using a square well potential term for NOE terms (100 kcal mol^{-1} Å^{-2}) and a square well quadratic energy function for the torsional potential (500 kcal mol^{-1} rad^{-1}). A force constant of 1,000 kcal mol^{-1} Å^{-2} was used for covalent bonds.

MT2s as well as between the N- and C-terminal domains of mouse MT1.

The slowly exchanging amide protons, as measured by H_2O vs. D_2O exchange, are tabulated in Table 3 for mouse MT1 and human MT2. The enhanced flexibility of the β-domain compared to the α-domain in both isoforms is immediately apparent, with only one slowly exchanging backbone amide proton in human MT2 and none in mouse MT1. The only slowly exchanging amide protons in the β-domain of mouse MT1 are the side-chain NH_2 protons of Asn23. Human MT2 contains a glutamate residue at this position, rendering a direct comparison impossible. Despite some differences in the number and position of the slowly exchanging protons in the α-domain, it can be concluded that the general trend is similar in the C-terminal domains of both human MT2 and mouse MT1.

The cadmium–cadmium exchange in mouse MT1 was analyzed by a modified HSQC-type pulse sequence (Fig. 6), where the cadmium signals were selectively saturated after transfer of magnetization from the attached protons, and the reduction of magnetization of the other cadmium signals monitored. This indirect detection of cadmium exchange was used due to its increased sensitivity over direct ^{113}Cd detection. A one-dimensional ^{113}Cd saturation transfer experiment has been described by Otvos et al. (1987) for rabbit MT2, and the results are compared in Table 4. As can be seen, the cadmium–cadmium exchange in the β-domain is much faster in mouse-MT1 than in human MT2. The cadmium signals in the α-domain of both proteins do not decay upon saturation of the other α-domain cadmium signals reflecting a much slower Cd chemical exchange in the C-terminal four-metal cluster.

Discussion

In every metallothionein structural study described in the literature, the number of NOEs in the β-domain is lower than in the α-domain. Mouse metallothionein-1, however, showed by far the largest difference in numbers of NOEs between the two domains (Table 5). The ratio of NOEs in the β- vs. the α-domain is 0.37 for all NOEs and 0.28 for interresidual NOEs in mouse MT1, whereas

Table 3. *List of slowly exchanging amide protons in mouse MT1 and human MT2*[a]

Amide proton exchange rates		
	Exchange rates (min^{-1})	
Residue	Mouse [Cd_7]-MT1	Human [Cd_7]-MT2[b]
	β-Domain	
C21	n.o.[c]	1×10^{-1}
N23 NH_2 a[d]	1.4×10^{-2}	n.a.[f]
N23 NH_2 b[e]	1.7×10^{-2}	n.a.[f]
	α-Domain	
C36	n.o.[c]	2.0×10^{-1}
C37	1.4×10^{-2}	2.0×10^{-2}
C44	3.2×10^{-3}	4.8×10^{-4}
A45	1.2×10^{-2}	6.2×10^{-2}
Q46	7.1×10^{-3}	n.o.[c]
G47	1.1×10^{-2}	n.o.[c]
V/I49[g]	n.o.[c]	3.0×10^{-3}
C50	4.5×10^{-5}	5.6×10^{-4}
G52	1.2×10^{-2}	n.o.[c]

[a] The exchange rates were measured by dissolving the protonated protein in D_2O and monitoring the decay of signals as a function of time. The only slowly exchanging signals found in the β-domain are at Cys21 of human MT2 and the side-chain amide protons at position Asn23 of mouse-MT1.
[b] Messerle et al. (1990a).
[c] Not observed.
[d] Side-chain NH_2 resonance at 6.91 ppm.
[e] Side-chain NH_2 resonance at 7.60 ppm.
[f] In human MT2 there is a glutamate residue at position 23.
[g] A valine residue is at position 49 in mouse MT1 and an isoleucine in human MT2.

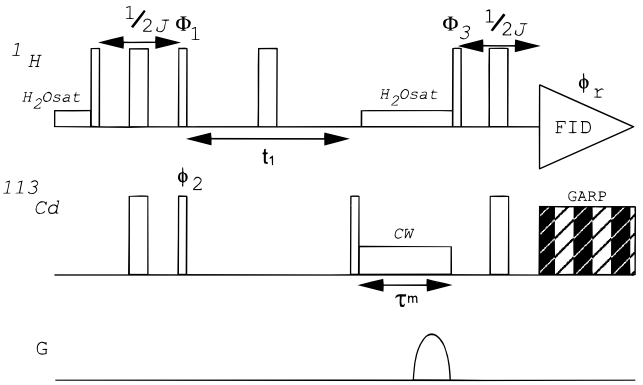

Fig. 6. Modified HSQC-type pulse sequence, which allowed saturation transfer between the signals in the indirect dimension. After the excitation of proton magnetization and antiphase polarization transfer to the heteronucleus, the chemical shift of the latter can evolve during t_1. Subsequently, longitudinal two-spin order magnetization (I_zS_z) is produced by a 90° ^{113}Cd pulse, and in the following mixing time specific cadmium signals can be selectively decoupled. Another 90° ^{113}Cd pulse creates antiphase magnetization again, which is then transferred to the protons and detected. Thin and thick bars represent 90° and 180° pulses, respectively. The abbreviations are as follows: H_2Osat, saturation delay to suppress the solvent signal; τ_m, mixing time; CW, continuous wave saturation; GARP, GARP decoupling of cadmium during acquisition. The following phase cycling was used: $\phi_1 = y,y,-y,-y$; $\phi_2 = x,-x$; $\phi_3 = x,x,x,x,-x,-x,-x,-x$; $\phi_r = x,-x,-x,x,-x,x,x,-x$; all other phases are x. Unwanted magnetization terms during the mixing period are destroyed by a gradient pulse after the saturation period.

in other MTs studied these numbers are around 0.75 and 0.65, respectively. Because the average structure of the β-domain of mouse MT1 is very similar to the β-domains of other MTs (Fig. 7), the lower number of NOEs is most likely related to increased structural mobility. This assumption is corroborated by the absence of the single slowly exchanging backbone amide proton and the faster cadmium–cadmium exchange rates in the β-domain of mouse MT1 compared to MT2s (Table 4).

A comparison of the energy-minimized average backbone structure of both domains to the respective domains of rat MT2 (Fig. 7) shows a high degree of structural similarity of both domains of these proteins. The RMSD of these superimpositions is 1.94 Å for the β-domains and 2.14 Å for the α-domains. As can be seen in Figure 7, the loop between residues 52 and 57 in the α-domain is closer to the loop between residues 34 and 37 in mouse MT1 than it is in rat MT2. Steric hindrance between the side chains of Glu52 and Lys51 in rat MT2 presumably restricts such an arrangement as seen in mouse MT1, which has a glycine residue at position 52. The number and position of the slowly exchanging amide protons in the α-domain of mouse-MT1 and human-MT2 are also indicative of a similar structure of this domain. The slow exchange of the side-chain NH_2 protons of Asn23 of mouse-MT1 is indicative of a hydrogen bond. The carbonyl oxygen atoms of both Ser28 and Cys29 are close to these amide protons, and either one or both of them might be involved in a hydrogen bond.

The main difference in the amino acid sequence of MT2s and MT1s is reflected in the number of charged residues. Compared to rat liver MT2 (Schultze et al., 1988), mouse MT1 has two less negative (residue 10 and 52) and one less positive (residue 20) charges. This could only result in reduced electrostatic interactions in MT1 relative to MT2, which may account for the increased flexibility of the β-domain of MT1, which has two charges less than

Table 4. *List showing the percentage reduction of the cadmium signals after saturating another cadmium resonance*[a]

Saturation transfer between cadmium resonances in the β-domain			
Saturated Cd	Observed Cd	Rabbit MT2[b,c] (%)	Mouse MT1[d] (%)
CdII	CdIII	58	65
	CdIV	28	70
CdIII	CdII	58	51
	CdIV	32	59
CdIV	CdII	17	72
	CdIII	10	76

[a] Otvos et al. (1987) applied saturating fields for a couple of seconds before acquiring one-dimensional ^{113}Cd spectra of rabbit MT2. An HSQC-type experiment (see text) was used to obtain this percentage in mouse MT1.
[b] Otvos et al. (1987).
[c] Saturation time >1 s.
[d] Saturation time 100 ms.

Table 5. *Comparison of the number of NOEs found in various metallothioneins* [a]

	β-Domain		α-Domain		β-Domain/α-domain	
	Total	Interresidue	Total	Interresidue	Total	Interresidue
Mouse MT1	103	49	278	177	0.37	0.28
Human MT2[b]	116	78	144	117	0.81	0.67
Rabbit MT2[c]	n.a.[d]	49	n.a.[d]	80	n.a.[d]	0.61
Rat MT2[e]	n.a.[d]	46	n.a.[d]	80	n.a.[d]	0.58
Crab MT1[f]	115	n.a.[d]	163	n.a.[d]	0.71	n.a.[d]

[a] Although the total number of NOEs found in this study of mouse metallothionein-1 is higher than any other MT described in the literature, there are about as many NOEs in the β-domain of mouse MT1 compared to other MTs. The ratio of NOEs in the β-domain vs. the α-domain as shown in the last two columns clearly indicates that the number of NOEs per residue is unproportionally higher in the α-domain compared to the β-domain of mouse-MT1.
[b] Messerle et al. (1990b).
[c] Arseniev et al. (1988).
[d] Not available from the corresponding publication.
[e] Schultze et al. (1988).
[f] Narula et al. (1995).

in MT2. The electrostatic potential surface of the X-ray structure of rat MT2 (Robbins et al., 1991) shows the two domains to be slightly bent toward each other presumably as a result of the opposite and attractive charges of the two domains (Lys20, Lys22, and Lys31 on the β-domain and Glu52 and Asp55 on the α-domain) (Fig. 8). The strength of this interdomain attraction would be reduced in MT1, which has one less positive charge at residue 20 and one less negative charge at residue 52. Unfortunately, the absence of interdomain NOEs in both isoforms does not permit the relative orientation of the two domains to be established by homonuclear two-dimensional ^{1}H-NMR spectroscopy. Therefore, we can only suggest that the higher flexibility of the β-domain in mouse MT1 results in part from the reduced electrostatic attractions within and between the two domains compared to MT2.

Materials and methods

Sample preparation

Recombinant mouse MT1 was expressed from a pET3d vector (Novagen, Madison Wisconsin) in the *Escherichia coli* BL21(pLysS) strain. $ZnCl_2$ was added after induction with IPTG (Erickson et al., 1994). The protein was purified first by a Sephadex G75 gel filtration column, and the collected Zn^{2+}-containing fractions were loaded onto a DE-32 anion exchange column and eluted with a Tris-HCl gradient (Li & Otvos, 1996). The combined MT1 containing fractions were concentrated in an Amicon (Beverly, Massachusetts) apparatus fitted with a YM-3 membrane under nitrogen pressure. The ^{113}Cd-enriched protein was obtained by the mass action exchange of Zn^{2+} by the addition of an eightfold excess of $^{113}CdCl_2$, incubation for 5 min, and removal of the excess metal ions by Chelex-100. The sample was concentrated in an Amicon apparatus, and the buffer changed to 15 mM KPi pH 6.5, 0.02% NaN_3, and 10% D_2O was added for field-frequency lock.

NMR methods

Spectra were recorded on either an 800 MHz Varian Unity INOVA (^{1}H homonuclear spectra) or a 600 MHz Varian Unity INOVA (^{1}H-^{113}Cd HMQCs). All the measurements were performed on a sample containing 0.5 mL of protein at a concentration of 0.7 mM in a high precision 5 mm NMR sample tube. Due to the high flexibility of mouse MT1 and, therefore, increased amide proton and cadmium–cadmium exchange rates, spectra were acquired at 10 °C. Spectra at 25 °C were recorded to resolve remaining degeneracies. All of the two-dimensional spectra were acquired in the phase-sensitive mode, using the States–Haberkorn method (States et al., 1982). The carrier was always set on the solvent signal in all the homonuclear experiments because the solvent was suppressed using the watergate sequence (Piotto et al., 1992). The spectra were referenced against the temperature-corrected chemical shift of water, which is 4.945 ppm at 10 °C and 4.766 ppm at 25 °C (Wishart et al., 1995). For each of the 256 t_1 increments of 2k complex data points, 32 transients were collected for the NOESY

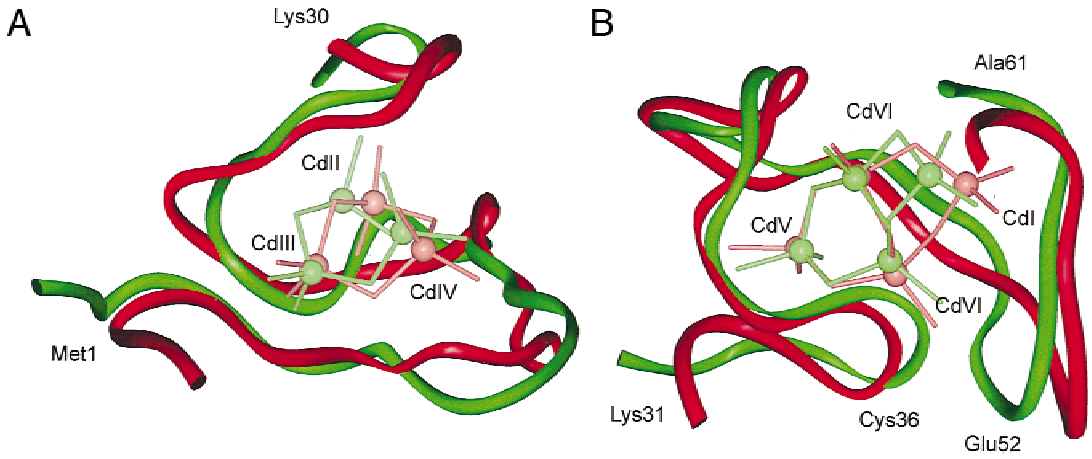

Fig. 7. Least-squares superposition of the backbones and cadmium–sulfur cluster of each domain of mouse MT1 (green) and rat MT2 (red) displayed in a tube drawing. **A:** The energy-minimized average structure of the β-domain. **B:** The α-domain. Due to steric hindrance of the side chains of Glu52 and Lys51 in rat MT2, the loop containing residue 52 is closer to the loop containing residue 36 in mouse MT1 (see text for details).

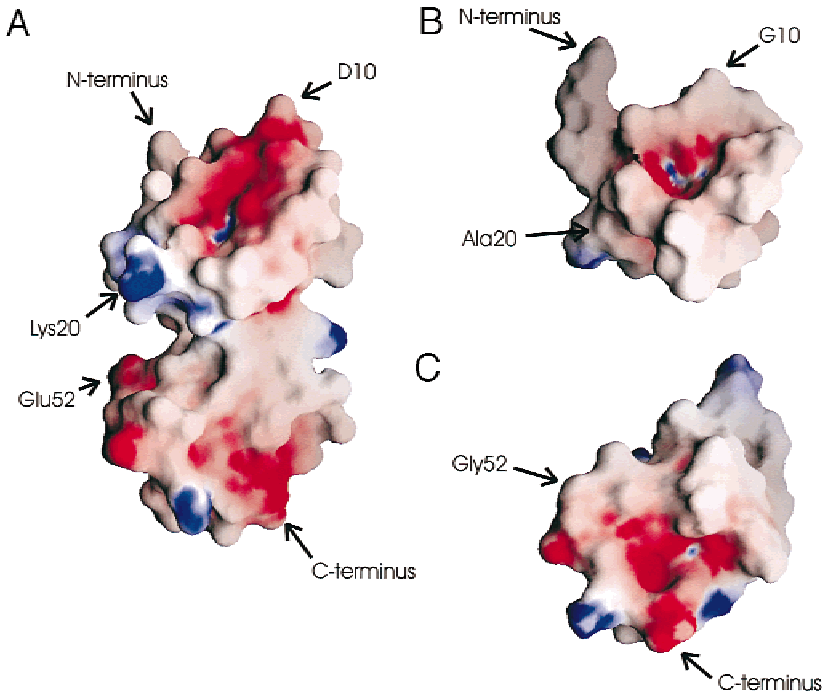

Fig. 8. Surface plot of the electrostatic potential of the crystal structure of (**A**) rat MT2 and the energy-minimized average structure of the (**B**) β-domain as well as (**C**) α-domain of mouse MT1 in the same orientation. Positive potentials are shown in blue; negative ones in red. Differences in the amino acid sequence that give rise to changes in the electrostatic potential surface are indicated and so are the N- and C-termini.

(Jeener et al., 1979) and TOCSY (Braunschweiler & Ernst, 1983) spectra. The data matrices were zero filled in F_1 to the final size of 2k $*$ 1k, and multiplied by 60° phase-shifted squared cosine window functions in both dimensions prior to Fourier transformation. Mixing times of 50, 100, and 150 ms were used for the NOESY spectra, and TOCSY spectra were recorded with mixing times of 30 and 60 ms. A DIPSI-2 (Shaka et al., 1988), spin-lock field with a power of 15 kHz, was used for the TOCSY experiments. Due to the wide range of ^{1}H-^{113}Cd coupling constants in metallothioneins (usually between 5 and 50 Hz), a set of HMQC (Müller, 1979) or HSQC (Bodenhausen & Ruben, 1980) spectra with varying preparation delays, corresponding to $1/2J^{H\text{-}Cd}$ is usually acquired. However, to obtain a single spectrum, which shows all the cysteine–cadmium correlations, we have used the accordion-HMQC experiment (Zangger & Armitage, 1999). The preparation time in this experiment was systematically incremented between 10 and 100 ms, which corresponds to coupling constants between 5 and 50 Hz. Due to the narrower solvent signal and, therefore, more efficient water suppression, this experiment was performed at 25 °C. Cadmium decoupling during the acquisition was performed by a GARP pulse cluster (Shaka et al., 1985).

Slowly exchanging amide protons were determined by lyophilization of a solution of the protein in H_2O, followed by solubilization in D_2O and monitoring of the amide signals as a function of time. Cadmium–cadmium exchange was analyzed by the pulse sequence in Figure 6. After the transfer of magnetization from the protons to the attached cadmiums and the evolution time t_1, longitudinal two-spin order terms I_zS_z were created by a 90° cadmium pulse and during the subsequent mixing time of 100 ms each cadmium signal was selectively saturated. Antiphase cadmium magnetization was subsequently generated again and transferred to the protons and monitored in phase-sensitive mode.

Structure calculations

All structure calculations were performed with the program X-PLOR 3.851 on a SGI IRIS Indigo Impact 10000 computer. Because there are no interdomain NOEs between the N-terminal β-domain and the C-terminal α-domain, the structures of the two domains were calculated separately. With the established cysteine–cadmium connectivities, new cadmium–sulfur cluster residues were defined within X-PLOR (Brünger et al., 1986) with the stoichiometries Cd_4S_{11} (α-domain) and Cd_3S_9 (β-domain). Information about the cadmium–sulfur bond lengths, as well as Cd-S-Cd, S-Cd-S, and CysC^{β}-S-Cd bond angles was taken from the X-ray crystal structures of model cadmium complexes and rat liver Cd_5Zn_2MT2 (Lacelle et al., 1984; Watson et al., 1985; Robbins et al., 1991). The following force constants were used: sulfur–cadmium bonds: 500 kcal mol^{-1} $Å^{-2}$; cadmium–sulfur–cadmium and sulfur–cadmium–sulfur angles: 250 kcal mol^{-1} rad^{-2}.

A total of 278 NOEs for the α-domain and 103 NOEs for the β-domain were used for the structure calculation. The lack of structural rigidity and chemical exchange contributions to the line widths made the extraction of coupling constants from two-dimensional COSY (Aue et al., 1976) type datasets unreliable. Therefore, no experimental dihedral angle constraints were used for the structure calculation. The NOEs were classified as strong, medium, and weak, corresponding to lower and upper distance limits of 1.8–2.7, 1.8–3.3, and 1.8–5.0 Å, respectively, for the α-domain (Williamson et al., 1985). Due to the overall lower intensity of cross peaks throughout the β-domain, the limits here were set to 1.8–2.5, 1.8–3.0, and 1.8–4.5 Å for, strong, medium, and weak peaks, respectively. For all the NOEs that involved methyl groups, 0.5 Å was added to the upper distance limit (Clore et al., 1987). The lower limit of 1.8 Å is the sum of the van der

Waals radii of two protons. The hybrid distance geometry-dynamical simulated annealing protocol (Nilges et al., 1988) was used for the calculation of structures. An initial covalent starting structure in distance space was created. From this structure, a family of 50 embedded substructures was produced using the substructure distance geometry approach and all the experimental NOE constraints. After an initial Powell minimization, these structures were optimized by simulated annealing and further Powell minimization. The target function during the simulated annealing contains only quadratic harmonic terms for bonds, angles, planes, and chirality, and square well quadratic terms for the experimental distance constraints and a quadratic van der Waals term for nonbonded interactions. Due to the limited number of NOE constraints, the force constant for NOEs was set to 100 kcal mol^{-1} $Å^{-2}$, instead of 50 kcal mol^{-1} $Å^{-2}$, which is usually used. Finally, the structures were further refined with simulated annealing with a reduced number of cooling steps. All structures that showed no more than one NOE violation greater than 0.5 Å, an RMS difference for bond deviations from ideality of less than 0.01 Å, and an RMS difference for angle deviations from ideality of $<5°$ were selected as final structures. Using these criteria, of the 50 calculated structures, 39 were selected for the β-domain and 41 for the α-domain.

InsightII was used for the display of structures and GRASP (Nicholls et al., 1991) for calculating the electrostatic potential surfaces. The online program Jalview (http://circinus.ebi.ac.uk:6543/jalview) was used for calculating the sequence homologies between different MT isoforms.

Supplementary material in the Electronic Appendix

A table of ^{1}H chemical shifts of mouse metallothionein-1 at 10 °C pH 6.5. Ordering information is given on any current masthead page.

Acknowledgments

Partial support of this work comes from the NIH Grant DK18778 to I.M.A. K.Z. thanks the Austrian Fonds zur Förderung der wissenschaftlichen Forschung for an Erwin Schrödinger Fellowship (project numbers J-1393CHE and J-1618CHE). NMR instrumentation was provided with funds from the NSF (BIR-961477) and the University of Minnesota Medical School. We also thank the Minnesota Supercomputer Institute (MSI) for the use of their computers for structural calculations and Ms. Qun Zhou for help in the protein purification.

References

Arseniev A, Schultze P, Wörgötter E, Braun W, Wagner G, Vašak M, Kägi JHR, Wüthrich K. 1988. Three-dimensional structure of rabbit liver [Cd_7] metallothionein-2a in aqueous solution determined by nuclear magnetic resonance spectroscopy. *J Mol Biol 201*:637–657.

Aue WP, Bartholdi E, Ernst RR. 1976. Two-dimensional spectroscopy. Application to nuclear magnetic resonance. *J Chem Phys 64*:2229–2246.

Binz PA, Kägi JHR. 1999. Metallothionein: Molecular evolution and classification. In: Klaassen CD, ed. *Metallothionein IV*. Basel: Birkhäuser Verlag. pp 7–13.

Bodenhausen G, Ruben DJ. 1980. Natural abundance nitrogen-15 NMR by enhanced heteronuclear spectroscopy. *Chem Phys Lett 69*:185–188.

Braunschweiler L, Ernst RR. 1983. Coherence transfer by isotropic mixing. Application to proton correlation spectroscopy. *J Magn Reson 53*:521–528.

Brünger AT, Clore GM, Gronenborn AM, Karplus M. 1986. Three-dimensional structures of proteins by molecular dynamics with interproton distance Restraints: Application to crambin. *Proc Natl Acad Sci USA 83*:3801–8305.

Clore GM, Gronenborn AM, Nilges M, Ryan CA. 1987. Three-dimensional structure of potato carboxypeptidase inhibitor in solution. A study using nuclear magnetic resonance, distance geometry, and restraint molecular dynamics. *Biochemistry 26*:8012–8013.

Erickson JC, Sewell AK, Jensen LT, Winge DR, Palmiter RD. 1994. Enhanced neurotrophic activity in Alzheimer's disease cortex is not associated with down-regulation of metallothionein-III (GIF). *Brain Res 649*:297–304.

Jeener J, Meier BH, Bachmann P, Ernst RR. 1979. Investigation of exchange processes by two-dimensional NMR spectroscopy. *J Chem Phys 71*:4546–4563.

Kägi JHR, Kojima Y. 1987. Chemistry and biochemistry of metallothionein. In: Kägi JHR, Kojima Y, eds. *Metallothionein II*. Basel: Birkhäuser Verlag. pp 25–61.

Kägi JHR, Schäffer A. 1988. Biochemistry of metallothionein. *Biochemistry 27*:8509–8515.

Lacelle S, Steven WC, Kurtz DM, Richardson JW, Jacobson RA. 1984. Crystal and molecular structure of $[Cd_{10}(SCH_2CH_2OH)_{16}](ClO_4)_4 \cdot 8H_2O$, Correlation with ^{113}Cd NMR spectroscopy of the solid and implications for cadmium-thiolate ligation in proteins. *Inorg Chem 23*:930–935.

Li H, Otvos JD. 1996. ^{113}Cd NMR studies of the domain specificity of Ag^+ and Cu^+ binding to metallothionein. *Biochemistry 35*:13929–13936.

Messerle B, Bos M, Schäffer A, Vašak M, Kägi JHR, Wüthrich K. 1990a. Amide proton exchange in human metallothionein-2 measured by nuclear magnetic resonance spectroscopy. *J Mol Biol 214*:781–786.

Messerle B, Schäffer A, Vašak M, Kägi JHR, Wüthrich K. 1990b. Three-dimensional structure of human liver [Cd_7] metallothionein-2 in aqueous solution determined by nuclear magnetic resonance spectroscopy. *J Mol Biol 214*:765–779.

Messerle B, Schäffer A, Vašak M, Kägi JHR, Wüthrich K. 1992. Comparison of the solution conformation of human [Zn_7]-metallothionein-2 and [Cd_7]-metallothionein-2 using nuclear magnetic resonance spectroscopy. *J Mol Biol 225*:433–443.

Müller L. 1979. Sensitivity enhanced detection of weak nuclei using heteronuclear multiple quantum coherence. *J Am Chem Soc 101*:4481–4484.

Narula SS, Brouwer M, Hua Y, Armitage IM. 1995. Three-dimensional structure of callinectes sapidus metallothionein-1 determined by homonuclear and heteronuclear magnetic resonance spectroscopy. *Biochemistry 34*:620–631.

Nicholls A, Sharp K, Honig B. 1991. Protein folding and association: Insights from the interfacial and thermodynamic properties of hydrocarbons. *Proteins 11*:281–296.

Nilges M, Clore GM, Gronenborn AM. 1988. Determination of the three-dimensional structures of proteins from interprotons distance data by hybrid distance geometry-dynamical simulated annealing calculations. *FEBS Lett 229*:317–329.

Otvos JD, Engeseth HR, Nettesheim DG, Hilt CR. 1987. Interprotein metal exchange reactions of metallothionein. In: *Metallothionein II*. Basel: Birkhäuser Verlag. pp 171–178.

Piotto M, Saudek V, Sklenar V. 1992. Gradient-tailored excitation for single-quantum NMR spectroscopy of aqueous solutions. *J Biomol NMR 2*:661–665.

Robbins AH, McRee DE, Williamson M, Collet SA, Xuong NH, Furey WF, Wang BC, Stout CD. 1991. Refined crystal structure of Cd,Zn metallothionein at 2.0 Å resolution. *J Mol Biol 221*:1269–1293.

Schultze P, Wörgötter E, Braun W, Wagner G, Vašak M, Kägi JHR, Wüthrich K. 1988. Conformation of [Cd_7]-metallothionein-2 from rat liver in aqueous solution determined by nuclear magnetic resonance spectroscopy. *Biochemistry 203*:251–268.

Shaka AJ, Barker PB, Freeman R. 1985. Computer-optimized decoupling scheme for wideband application and low-level operation. *J Magn Reson 64*:547–552.

Shaka AJ, Lee CJ, Pines A. 1988. Iterative schemes for bilinear operators: Application to spin decoupling. *J Magn Reson 77*:274–293.

States DJ, Haberkorn RA, Ruben DJ. 1982. A two-dimensional nuclear Overhauser experiment with pure absorption phase in four quadrants. *J Magn Reson 48*:286–292.

Watson AD, Rao CP, Dorfman JR, Holm RH. 1985. Systematic stereochemistry of metal(II) thiolates; synthesis and structures of $[M_2\{SC_2H_5\}_6]^{2-}$ (M=Mn(II), Ni(II), Zn(II), Cd(II). *Inorg Chem 24*:2820–2826.

Williamson MP, Havel TF, Wüthrich K. 1985. Solution conformation of proteinase inhibitor IIA from bull seminal plasma by ^{1}H nuclear magnetic resonance and distance geometry. *J Mol Biol 182*:295–315.

Wishart DS, Bigam CG, Yao J, Abildgaard F, Dyson HJ, Oldfield E, Markley JL, Sykes BD. 1995. ^{1}H, ^{13}C and ^{15}N chemical shift referencing in biomolecular NMR. *J Biomol NMR 6*:135–140.

Wüthrich K. 1986. *NMR of proteins and nucleic acids*. New York: John Wiley & Sons.

Zangger K, Armitage IM. 1999. The accordion HMQC. Heteronuclear correlation for a range of coupling constants. *J Magn Reson*. Forthcoming.